*Sensors & Transducers, Vol. 236, Issue 8, August 2019, pp. 7-15*

**Sensors & Transducers**
Published by IFSA Publishing, S. L., 2019
http://www.sensorsportal.com

# A Damaged Twisted Pair Cable Modeling for Fault Detection and Characterization using OMTDR and Particle Swarm Algorithm

**[*] Wafa BEN HASSEN, Moussa KAFAL**
CEA, LIST, Laboratoire de Fiabilité et Intégration Capteurs, 91191 Gif-sur-Yvette, France
[*] E-mail: wafa.benhassen@cea.fr

*Received: 18 June 2019 /Accepted: 22 July 2019 /Published: 31 August 2019*

**Abstract:** This paper aims at developing algorithms permitting to detect, locate and characterize soft faults (i.e. isolation damage) in stranded unshielded twisted pair (SUTP) cables. To do so, a distributed parameters model of the SUTP cable including the pitch of twist, number of strands in addition to the skin and the proximity effects is developed. Once validated with 3D-electromagnetic simulations, a soft fault is modeled and its signature is detected and extracted using reflectometry. After that, a model inversion process relying on optimization-based methods (i.e. Particle Swarm) is deployed to characterize the soft fault. This latter permits to estimate the fault's dimensions (i.e. width, length, etc.) and its electrical parameters (i.e. capacitance, inductance, impedance, etc.) based on its electrical signature. More importantly, this would enable a close assessment of the remaining useful lifetime of the cable with the aid of datasheets provided by cable manufacturers.

**Keywords:** Reflectometry techniques, Transmission line networks, Soft fault detection and characterization, Particle swarm optimization algorithm.

## 1. Introduction

In aircrafts, electrical wiring networks form the backbone for energy and information exchange within its systems, with cumulated lengths exceeding tens of hundreds of Kms. However, airplanes are exposed to severe operational and environmental conditions (heating, humidity, vibration, etc.,) thus leading to the appearance of anomalies in cables. This can introduce loss of system functionalities leading in some cases to catastrophic crashes. Although, several electric and non-electric methods have been developed for the sake of detecting and locating wiring faults, reflectometry techniques have been and are still in the center stage of research and development. Essentially, based on a time-domain approach, reflectometry methods inject a test signal into the network under test (NUT) and monitor the reflected one in order to detect the presence, position, and nature of an impedance discontinuity [1]. For instance, standard time domain reflectometry (TDR) is based on a Dirac-pulse injection to recognize impedance discontinuities, thus the frequency spectrum of the injected signal is infinitely large, preventing this method from being suitable for embedded systems and distributed sensors networks. On the other hand, avoiding affecting the functionality of a system during live-diagnosis, specific methods based on the principles of OFDM (Orthogonal Frequency Division Multiplexing) have been developed under what is referred to as OMTDR (Orthogonal Multi-tone TDR) [2]. This technique have proven to provide a complete control of the spectrum of the injected signal which shall not interfere with the system under test. It does so by dividing the channel bandwidth into many sub-carriers independently modulated, hence providing a better spectral efficiency.

Although reflectometry has proven its efficiency to diagnose hard faults (i.e. open circuit and short circuit), it seems to be not sensitive enough to diagnose soft fault (e.g. shielding damage, pinching, etc.) [3]. In fact, this latter is characterized by a very small impedance variation that is translated on the corresponding reflectogram by a very weak signature. Add to that, the presence of heterogeneities along the NUT can locally create undesirable echoes and thus, increase the noise level on the reflectometry measurement, thus masking the signature of the eventual fault [4-5]. Moreover, the soft fault diagnosis performance may be disturbed by the attenuation and dispersion phenomena mainly present on long cables and become more critical in complex networks. Accordingly, with such constraints, the analysis of the corresponding reflectogram may be very complex and the soft fault diagnosis may be masked by noise. However, it is crucial to provide precise information on the fault to those who should accurately ensure system maintenance.

Within this context, the development and validation of the targeted NUT is very useful to predict the reflectometry response based on its characteristics (e.g. length, topology, electrical parameters, etc.) and its behavior with frequencies. This permits to provide the reference (reflectogram of the healthy cable) and to perform baselining to extract such weak soft fault signatures. Notwithstanding, the detection and location of soft faults is yet not sufficient in the perspective of predictive maintenance. In fact, the characterization of such faults by estimating their electrical parameters and dimensions would be more interesting. Despite of its good performance, reflectometry techniques alone do not permit to achieve this goal. On the other hand, if combined with data assimilation methods (e.g. Kalman filter) or optimization based algorithms (e.g. Genetic Algorithm (GA), Particle Swarm (PS), Artificial Neural Network (ANN), etc.), the objective can be attained.

This paper aims at developing algorithms permitting to detect, locate and characterize soft faults (i.e. isolation damage) in Stranded Unshielded Twisted Pair (SUTP) cables. To do so, a distributed parameters model including the pitch of twist, number of strands in addition to the skin and proximity effects [6] is developed. In the literature, most scientific references consider twisted pairs as parallel wire and replace air with uniform dielectric without considering the effect of twists on the characteristic impedance, coupling, and so on [7]. Moreover, stranded cables are, mostly, considered as a solid core. These assumptions are unsuitable, particularly, at high frequency since stranded cables have larger resistance compared to solid core ones [8].

Once validated with 3D-electromagnetic simulations, a soft fault is modeled and its signature is detected and extracted using reflectometry. After that, a model inversion relying on the merits of optimization-based methods (i.e. Particle Swarm) is deployed to characterize the soft fault. This latter permit to estimate the fault's dimensions (i.e. width, length, etc.) and its electrical parameters (i.e. capacitance, inductance, impedance, etc.) based on its electrical signature.

The remaining of the current paper is organized as follows: in Section 2, the distributed parameters model of a twisted pair is introduced. The validation of the developed model, in Section 3, is verified by 3D electromagnetic simulations. Section 4 proposes to study the behavior of the developed model of the twisted pair as a function of signal frequency, pitch of twist, and cable length. In Section 5, the detection and characterization of soft faults is introduced based on reflectometry and Particle Swarm. Section 6 evaluates the method's performance by using an OMTDR-based sensor for testing complex wiring networks in presence of an isolation damage.

## 2. Development of Distributed Parameters Model of a SUTP Cable

A SUTP is a transmission line composed of two stranded conductors spirally wound around each other to limit sensitivity to interference and cross-talk. It is widely used in the aeronautical field, for example, Controller Area Network (CAN) bus, MIL-STD-1553B, etc.

In this section, a model of a SUTP that resembles real cables found in the aeronautical field (for example the twisted pair EN 2267-010) is developed. Here, the twisted pair is composed of 19 strands per conductor. The diameter of a strand is $d_b$= 1/5 of the diameter of the conductor denoted $d$.

The characteristic impedance, $Z_c$, of a transmission line is a function of the distributed parameters (per unit length) series resistance $R$, series inductance $L$, shunt capacitance $C$, and shunt conductance $G$. The characteristic impedance is defined as follows:

$$Z_c = \sqrt{\frac{R + j\omega L}{G + j\omega C}} \quad (1)$$

The helical pitch angle of twist influences the dielectric constant denoted $\varepsilon_{eq}$ and is calculated in the Eq. (2) as follows [9]:

$$\theta = \tan^{-1}(2T\pi D), \quad (2)$$

where $T$ is the number of twists per meter and $D$ is the distance between two wires. The twist correction factor is then used to adjust the dielectric constant in the Eq. (3) as follows [7]:

$$q = 0.45 + 10^{-3}\left(\theta \frac{180}{\pi}\right)^2 \quad (3)$$

The dielectric constant integrating the influence of the twist angle $\varepsilon_{eq}$ can be calculated in Eq. (4) as follows [10]:

$$\varepsilon_{eq} = 1 + q(\varepsilon_r - 1), \quad (4)$$

where $\varepsilon_r$ is the relative permittivity. With the determined equivalent dielectric constant, the capacity can be described as:

$$C = \frac{\pi\varepsilon_0\varepsilon_{eq}}{log\left(\frac{D}{d}\right)}, \quad (5)$$

where $D$ is the distance between the two conductors. The parameter $\varepsilon_0$ is the permittivity of the air.

In the same way, the inductance per unit length of the cable is given in Eq. (6) by:

$$L = \frac{\mu_0\mu_r}{\pi}\, log\left(\frac{D}{d}\right), \quad (6)$$

where $\mu_0$ is the permeability of free space and $\mu_r$ is the relative permeability of the dielectric.

Since the reflectometry signal operates at high frequency to ensure accurate fault location, the developed model must reflect the behavior of the transmission line at such bands involving skin and proximity effects. In this paper, the proximity factor is noted $P$. It is determined according to the ratio between the distance between two conductors $D$ and the diameter of a conductor $d$ as described in [6].

For a twisted pair with 19 strands per conductor, one can calculate the resistance per unit-length in Eq. (7) (taking into account the proximity factor and the surface ratio of the conductor as a good approximation):

$$R(f) = P\left(\frac{19}{25}\right)\left(\frac{2}{\pi d\sigma\delta}\right), \quad (7)$$

where the skin effect d is expressed in Eq. (8) as follows:

$$\delta = \frac{1}{\sqrt{\pi d\sigma f}}, \quad (8)$$

$\mu = \mu_0\mu_r$ is the dielectric permeability, while $\sigma$ is conductor conductivity and $f$ is the frequency. The conductance per unit length $G$ is given in Eq. (9) as:

$$G = 2\pi f C \tan\delta, \quad (9)$$

with $\tan\delta$ being the tangent of dielectric loss and depends on the frequency.

## 3. Validation of the Distributed Parameters Model

In this section, it is proposed to validate the distributed parameters model described in Section 2. For this, the distance between the two conductors $D = 0.95mm$ and the diameter of a conductor $d = 0.75mm$. The strands are made of copper ($\sigma = 5.8107$ S/m ) and the insulator is made of Teflon ($\varepsilon_r$= 2.1 and $\mu = 4\pi 10^{-7}$). The proximity factor is P = 2.1 determined directly from the curve provided in [11] for a ratio $\left(\frac{D}{d}\right) = 1.2$. To reconstruct the reflectogram from the secondary parameters calculated on the basis of R, L, C and G, the transfer function expressed as follows can be used:

$$H(f) = \Gamma_E + \frac{(1-\Gamma_E^2)\Gamma_L e^{-2\gamma l}}{1+\Gamma_E\Gamma_L e^{-2\gamma l}}, \quad (10)$$

where $l$ is the length of the cable, $\Gamma_E$ is the reflection coefficient at the input of the line and $\gamma$ is the propagation constant. The propagation constant $\gamma$ is given by:

$$\gamma = \sqrt{(R + j\omega L)(G + j\omega C)} \quad (11)$$

The reflection coefficient $\Gamma_E$ at the input of the line is calculated as follows:

$$\Gamma_E = \frac{Z_c - Z_0}{Z_c + Z_0}, \quad (12)$$

with $Z_0$ is the impedance of the test signal generator. In this case, it is considered equal to 50Ω. In the case of an open circuit at the end of the line, the reflection coefficient in Eq. (10) is defined as $\Gamma_L = 1$.

To validate the developed model based on the distributed parameters defined in Eq. (5), Eq. (6), Eq. (7) and Eq. (9), a 3D model of the SUTP is developed using a dedicated 3D-electromagnetic simulations software as shown in Fig. 1. The model consists of 19 copper strands per conductor. The diameter of one strand is 0.15 mm. A thin layer of Teflon insulation covers the conductor. The thickness of this layer is 0.08 mm. The number of twist steps is 100 per meter. The length of the model is 1 m.

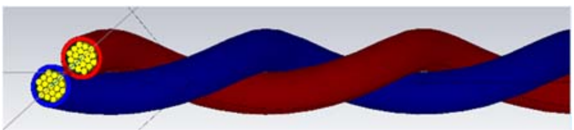

**Fig. 1.** The 3D electromagnetic model of a stranded USTP.

It is useful to compare the RLCG-based model and 3D-based model data in time domain since they are used for fault detection and location in SUTP. To do that, standard TDR is applied to analyze the transmission line behavior. Fig. 2 shows the TDR reflectograms of the RLCG-based model and the 3D-based model. The width of the Gaussian pulse injected as a testing signal is 1 ns. To compare the similarity between the data from the distributed parameters model and 3D electromagnetic simulations, this paper proposes to use the correlation coefficient. Here, it is considered that the data are strongly correlated if the correlation coefficient is between 0.9 and 1. In this context, the correlation coefficient between the two reflectograms resulting from the RLCG-based model and the 3D-based model is equal to 0.9855. One can thus consider that the correlation coefficient is strong and can thus validate the model with distributed constants developed in Section 2 in the case of a stranded twisted pair. The amplitude of the peak of the open circuit present at the end of the cable is equal to 0.86 V knowing that the amplitude of the Gaussian pulse is 1 V. The distributed parameters model will be used later for soft fault characterization.

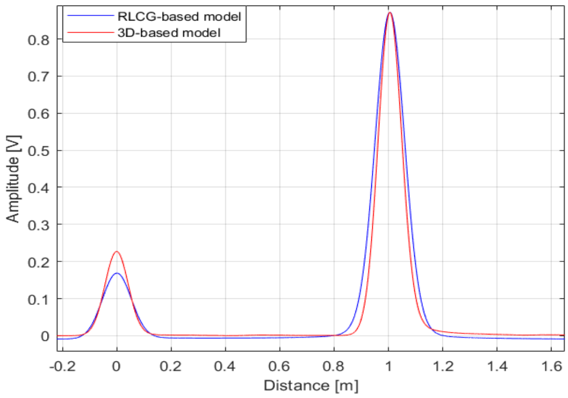


**Fig. 2.** TDR reflectograms of the distributed and 3D models.

## 4. Study of the Behavior of the Distributed Parameters Model

After the RLCG-model validation, the current section proposes to study the behavior the SUTP in frequency domain with respect to the same configuration introduced in Section 3.

Fig. 3 (top) and (bottom) show, respectively, the increase of the resistance R according to Eq. (7) and of the conductance G as a function of frequency.

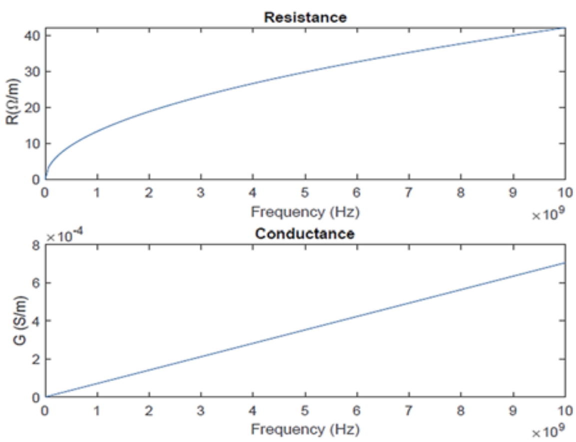


**Fig. 3.** Variation of the resistance R and the conductance G as a function of frequency.

The phase angle $\Phi(f)$ of the characteristic impedance of $Z_c(f)$ is given by:

$$\Phi(f)\text{=angle}\left(Re(Z_c(f)), Im(Z_c(f))\right)\frac{180}{\pi} \quad (13)$$

Fig. 4 (top) shows the modulus of the characteristic impedance as a function of the frequency and Fig. 4 (bottom) shows the phase of the characteristic impedance as a function of the frequency. The characteristic impedance is 71.4 Ω in this case study.

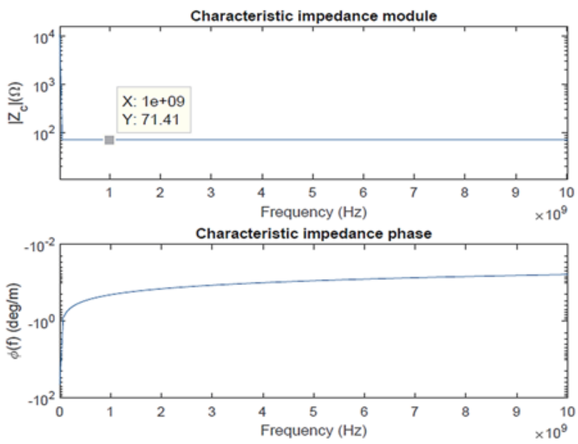


**Fig. 4.** Variation of the characteristic impedance $Z_c$ as a function of the frequency.

The attenuation of the cable in decibel/m is given as follows:

$$\alpha(f) = -20\log\left(Re\big(\gamma(f)\big)\right) \quad (14)$$

The phase constant in degree/m is given as follows:

$$\beta(f) = \frac{180}{\pi} Im\big(\gamma(f)\big) \quad (15)$$

Fig. 5 (top) and (bottom) show respectively the increase of the attenuation according to Eq. (14) and of the phase constant according to Eq. (15) as a function of frequency.

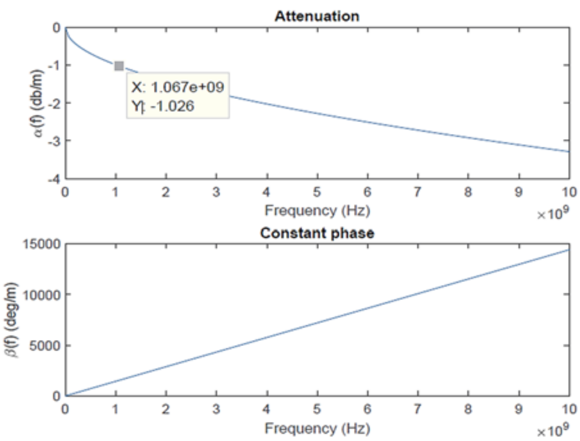


**Fig. 5.** Attenuation and phase constant versus frequency.

The frequency of the reflectometry signal is a critical parameter in detecting and locating a fault in a cable. Indeed, the higher the frequency is, the better the resolution of the reflectogram and the more accurate the localization of small defects. However, in the case of fault detection on long cables, increasing the signal frequency is not recommended as it introduces increase in signal attenuation. Indeed, TDR simulations were performed on the RLCG model of the twisted pair for a length of 100 m. In this context, the peak amplitude of the open circuit is 0.0084 V and 0.065 V for a frequency of 2 GHz and 200 MHz, respectively.

## 5. Isolation Damage Detection and Characterization

This section aims at developing an algorithm permitting to characterize soft faults (i.e. isolation damage) in SUTP cables. It permits to estimate the fault's dimensions (i.e. width, length, etc.) and its electrical parameters (i.e. capacitance, inductance, impedance, etc.) based on its electrical signature. A model inversion process based on optimization-based methods (i.e. Particle Swarm) permits to characterize and classify the soft fault.

### 5.1. Measurement of the Reflectometry Response of the Faulty UTP

A 5 mm isolation damage was created on the SUTP cable where three distinct isolation removals characterized by 42 %, 62 % and 100 % insulation cuttings were realized. Figs. 6, 7 and 8 show the corresponding models of soft faults denoted as $\boldsymbol{T_1}$, $\boldsymbol{T_2}$ and $\boldsymbol{T_3}$ respectively.

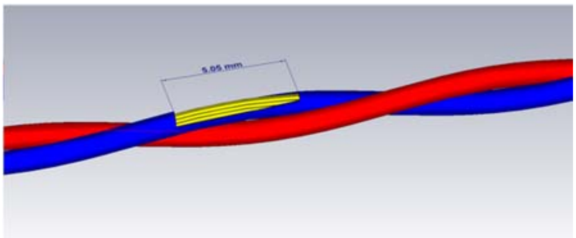

**Fig. 6.** Model of fault $T_1$.

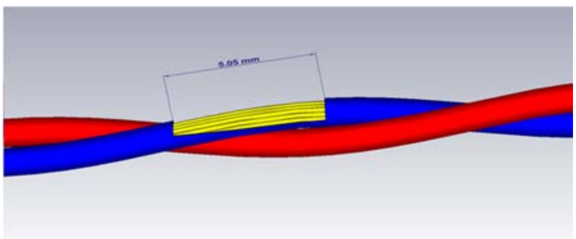

**Fig. 7.** Model of fault $T_2$.

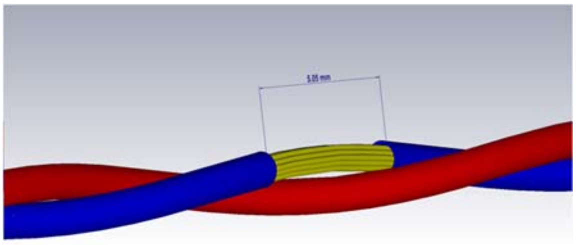

**Fig. 8**. Model of fault $T_3$.

Fig. 9 shows the baselined signatures of the models of faults $\boldsymbol{T_1}$, $\boldsymbol{T_2}$ and $\boldsymbol{T_3}$ where a difference operation, better known as baselining, is applied between the reflectometry responses of the faulty and healthy cases (reference). This permits to extract and amplify the signature of the soft fault and distinguish it from other impedances discontinuities such as splices, loads, etc.

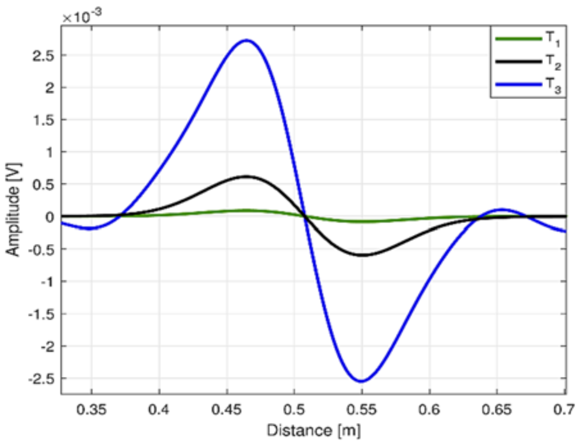


**Fig. 9.** Baselined signatures of the considered faults.

For these simulations, the maximum frequency of the signal is 1 GHz. It is obvious that the signature of the fault depends on the isolation damage severity. The first positive peak is at the 0.48 m while the second negative peak is at the 0.53 m corresponding to the 5 mm fault length. The amplitude of the differential signature of the fault $\boldsymbol{T_1}$ is 0.18 mV. The amplitude of the differential signature of the fault $\boldsymbol{T_2}$ is 0.61 mV. The amplitude of the differential signature of the fault $\boldsymbol{T_3}$ is 2.72 mV.

### 5.2. Application of the PSO to Estimate the Fault's Parameters

After soft fault detection using reflectometry, it is proposed to estimate its characteristics. To do so, an inverse problem should be solved, where optimization based techniques form an excellent candidate. The Particle swarm optimization (PSO) algorithm is considered in this paper thanks to its simplicity [12]. The principle of PSO algorithm is shown in Fig. 10.

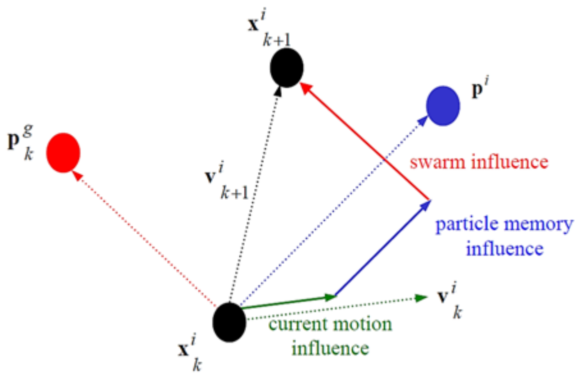


**Fig. 10.** A model demonstrating a particle's velocity and position updates in particle swarm optimization.

The population, often referred to as swarm, is composed of *n* candidate solutions known as particles. Each particle $i = 1,2,\cdots,n$ in the swarm space has an identity defined by its position $p_i$, in addition to its moving velocity $v_i$. In fact, the displacement of a particle in space is controlled by a well-defined strategy based on its own best known position $p_{best_i}$ as well as the global best known position $g_{best_i}$ of the entire swarm. It is important to note that, $\omega_i$ is the inertia weight specific to each particle, $r_1$ and $r_2$ are random numbers uniformly generated between [0; 1], while $c_1$ and $c_2$ are learning acceleration factors as follows:

$$v_i^{t+1} = \omega_i v_i^t + c_1 r_1^t \left(p_{best}{}_i^t - p_i^t\right) + c_2 r_2^t \left(g_{best}{}_i^t - p_i^t\right), \quad (16)$$

$$p_i^{t+1} = p_i^t + v_i^{t+1} \quad (17)$$

As an illustration, the particles' convergence towards the best solution is likely determined by their fitness that is controlled by a predefined objective function $F_{obj}$ specific to each application. Namely, the position $p$ determines each particle's fitness that is updated regularly at each iteration $t$ of the PSO algorithm according to what has been defined in Eq. (16) and Eq. (17). The process is repeated until a specific criterion is reached which might be the maximum number of iterations, the stalking state time after which no improvements can be detected, etc.

In our case, the proposed algorithm considers three set of variables or particles to run. The first set corresponds to the nature of the fault where a vector {N}={L} including the starting values (in the case of a healthy cable): the resistance R, the inductance L, and the capacitance C. The second set is the fault parameters $\{D\}=\{L_f, p_f\}$, where $L_f$ is the fault length and $p_f$ is the fault position. The last set of variables is the variation denoted $\Delta_v$ with respect to the RLCG parameters of the cable under test. Here, $\Delta_v$ is a vector of 1 element including the variation of L. The other parameters R, C and G variations are not considered in this study. At the output, one can define, for example, the resistance of the fault $L_d = L(1 + \Delta_v(1)/100)$.

The assigned objective function is given by Eq. (18), where $V(t)_{mes}$ and $V(t)_{sim}$ are the time domain measured and simulated reflecometry responses. On the other hand, the stopping criteria is determined by a stalking time during after which no significant change in the population is noticed [13].

$$F_{obj} = \int_{t=0}^{\infty} \frac{\|V(t)_{sim} - V(t)_{mes}\|_2}{1 + t^2} \quad (18)$$

In this case, $V(t)_{mes}$ is the TDR-based reflectogram obtained using the 3D-models as shown in Fig. 9. $V(t)_{sim}$ is the TDR-based reflectogram obtained using the RLCG-based reflectogram accroding to Eq. (10).

In the case of fault $T_1$ where 42 % of the isolation is damaged with exposing the conductor over 5 mm, the variation of the inductance L noted $\Delta_v(1)$ is 0.74 %. The fault length is $l_f = 4.5$ mm and the fault position $p_f = 508$ mm. Based on the electrical fault's parameters obtained from the PSO algorithm such as the inductance $L_d$, the impedance of this fault is $Z_d = 71.76\Omega$ while the impedance of the healthy cable $Z_c = 71.501\Omega$. Fault $T_1$ thus introduces an impedance variation $0.26\Omega$ and hence, a reflection coefficient $\Gamma = (Z_d - Z_c)/(Z_d + Z_c) = 0.18 \times 10^{-2}$. Fig. 11 shows the reconstructed signature of the fault $T_1$ based on its estimated parameters according to PSO algorithm.

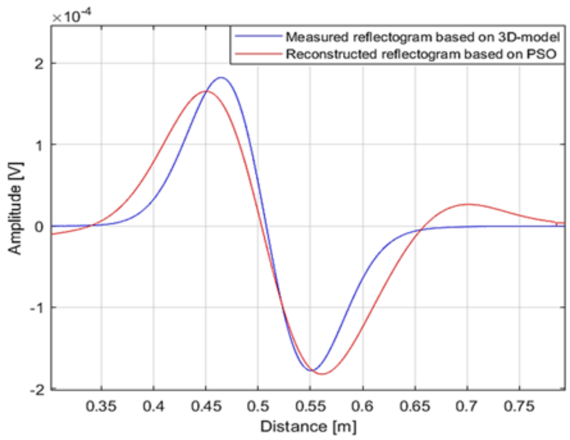


**Fig. 11.** Comparison between measured and reconstructed signature of fault $T_1$.

Table 1 summarizes the L parameter variation for faults $T_1$, $T_2$, and $T_3$ with length L =5 mm. The parameters R, C and G are considered constant in this study.

**Table 1.** The estimated parameters of the isolation damages.

| Fault | ΔL % | $p_f$ | $l_f$ | $\Delta Z_c$ |
|---|---|---|---|---|
| $T_1$ | 0.74 | 508 mm | 4.5 mm | 0.26 Ω |
| $T_2$ | 1.65 | 508 mm | 4 mm | 0.47 Ω |
| $T_3$ | 18.21 | 507 mm | 4.4 mm | 6.23 Ω |

It is possible to notice that the increase of the isolation damage causes an increase in variation of the inductance and hence, the characteristic impedance of a cable in the defective zone.

## 6. Experimental Results

The development of distributed parameters model permits to evaluate the reflectometry response in different configurations and thus to avoid the test bench performing leading to gain in cost and time. For experimental results, a 10 m long UTP EN 2267-009 DRB 24 is connected to an electronic board named “Ariane V2” that permits to inject/receive OMTDR signals. The electronic board includes FPGA SoC Xilinx ZyNQ 7010, 10-bits ADC, 10-bits DAC and 512 Megabyte DDR chip as shown in Fig. 12.

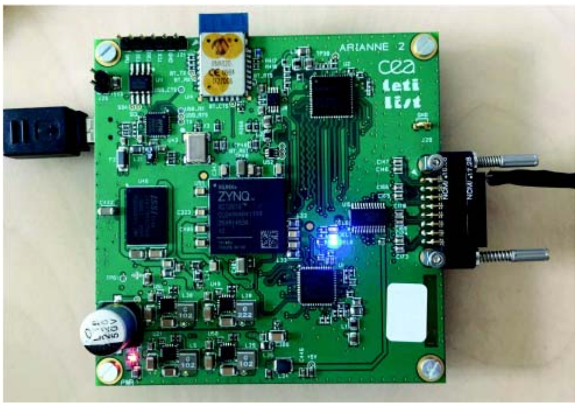


**Fig. 12.** TDR reflectograms from the RLCG model of the twisted pair at different frequencies.

An OMTDR based signal composed of 128 subcarriers over a total bandwidth (BW) ranging from 300 kHz to 1.5 GHz with 2048 frequency samples has been generated and injected into the tested network. The principle of OMTDR is shown in Fig. 13. The interested reader can go to [14] for more details concerning the OMTDR bloc’s functioning.

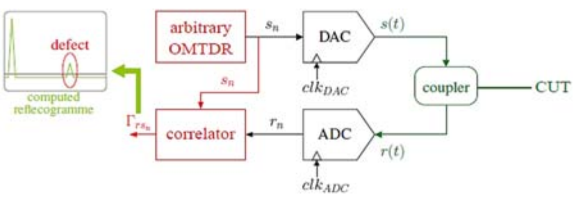


**Fig. 13.** Schematic diagram of an OMTDR reflectometry.

For simulation results, the processing realized by the electronic board named “Ariane V2” is modeled using Matlab simulations (i.e. analog to digital conversion, digital to analog conversion, oversampling, measurement noise, etc.). Fig. 14 shows the OMTDR based reflectogram of the model of SUTP cable and the measured one. The open circuit present at the end of the cable is represented on the reflectogram by an amplitude peak 0.36 with respect to the amplitude of the peak at the input of the reflectogram. In the same configuration, the open circuit present at the end of the cable with 100 m-length is represented on the reflectogram by a peak of amplitude 0.03 with respect to the amplitude of the peak at the entrance the reflectogram.

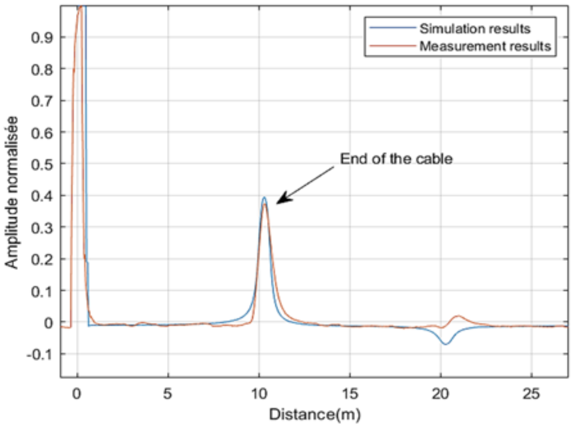


**Fig. 14.** OMTDR reflectograms of the RLCG model of the twisted pair 30 m long.

For complex network, the considered topology configuration of Fig. 15 was implemented using SUTP EN 2267-009 DRB 24. The extremities of the network were left open and one extremity served as a testing port. The branched network consists of 5 branches and 2 junctions. Fig. 16 shows the OMTDR reflectogram of the model of SUTP in the considered complex network.

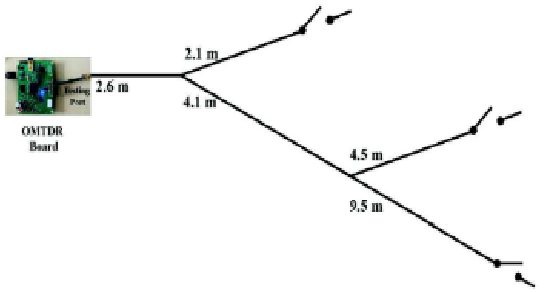


**Fig. 15.** OMTDR reflectograms of the RLCG model of the twisted pair 30 m long.

The distributed-constant model of the twisted pair may be extended to other twisted pairs. It suffices to define the geometrical properties (for example, conductor radius, distance between two conductors, etc.) and the electrical properties (for example, the permittivity of the insulator, the conductivity of the material, etc.) to determine the primary and subsequently secondary parameters. It is then sufficient to define the topology of the cable network to evaluate the performance of the on-board diagnostic system, and this in the desired configuration (presence of a connector, splice, etc.).

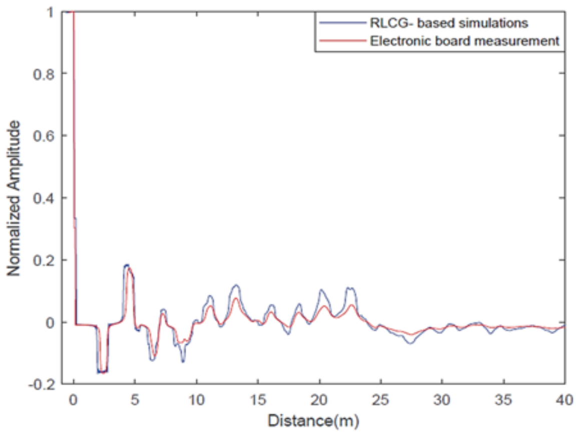


**Fig. 16.** The measured and simulation OMTDR responses of the tested NUT.

After validation of the developed NUT model based on experimental results, it is proposed to introduce an isolation damage $(T_1, T_2, T_3)$on the first branch at 1 m from the electronic board. Fig. 17 shows the OMTDR-based reflectograms in presence of different isolation damages that have been characterized later. Here, baselining is used to extract the soft fault signature from other impedance discontinuities on the NUT. It is obvious that the detection and location of the fault $T_3$ is possible in this configuration. However, the detection of the less severe faults where a part of the isolation is damaged such as $T_1$ and $T_2$ seems to be difficult.

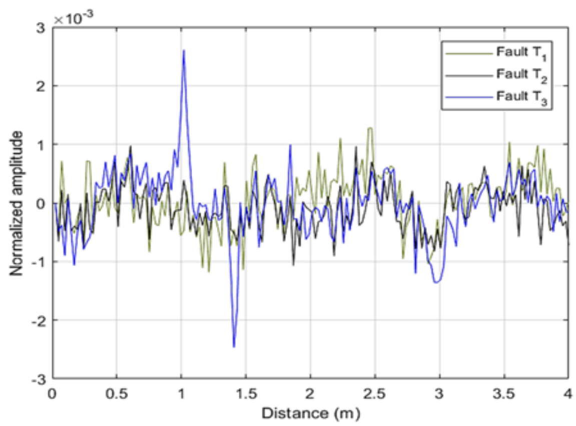


**Fig. 17.** OMTDR-based reflectograms with baselining in presence of isolation damages.

The characterization of the soft fault permits to predict its behavior in different configurations (position, frequency, network topology, etc.), and to evaluate the performance of the diagnosis systems in such fault detection and location.

The partial isolation damage is characterized by a very low impedance variation and then a low reflection coefficient and is rapidly masked by the attenuation and noise measurement. In this study, only the electrical phenomenon of the chafing is modeled and the electro-mechanical one is neglected. However, the isolation damage is mainly combined with pinching in practice, which introduces variation of the conductors' diameters and the angle twist in the case of the twisted pair cables. It seems to be important to include this latter to consider cases that are more realistic and study the effect of such combination on the soft fault characteristics.

## 7. Conclusions

This paper presented an extended study of [15] where a distributed parameters model of a shielded stranded twisted pair has been introduced. This model has been validated by 3D electromagnetic simulations. The developed model could be extended to other twisted pairs subject to knowing their geometric and electrical properties. This model permits to evaluate the diagnosis system (i.e. electronic board, etc.), in the desired configuration of a twisted pair without resorting to the establishment of a test bench. Moreover, the modeling of an isolation damage and its characterization using PSO algorithm permits to predict the performance of the diagnosis system to detect and locate such fault and thus enable predictive maintenance.

## References

[1]. F. Auzanneau, Wire troubleshooting and diagnosis: Review and perspectives, *Progress in Electromagnetics Research*, Vol. 49, 2013, pp. 253–279.

[2]. W. Ben Hassen, F. Auzanneau, L. Incarbone, *et al.*, Distributed sensor fusion for wire fault location using sensor clustering strategy, *International Journal of Distributed Sensor Networks*, Vol. 11, Issue 4, 2015.

[3]. M. Kafal, Jaume Benoit, Baselining: A critical approach used for soft fault detection in wire networks, *International Journal of Digital Information and Wireless Communications (IJDIWC)*, Vol. 8, Issue 1, 2018, pp. 52-57.

[4]. L. A. Griffiths, R. Parakh, C. Furse, B. Baker, The invisible fray: A critical analysis of the use reflectometry for fray location, *IEEE Sensors J.*, Vol. 6, Issue 3, Jun. 2006, pp. 697–706.

[5]. A. Cozza, Lionel Pichon, Echo response of faults in transmission lines: Models and limitations to fault detection, *IEEE Trans. on MTT*, Vol. 64, Issue 12, 2016, pp. 4155-4164.

[6]. K. Ferkal, M. Poloujadoff, E. Dorison, Proximity effect and eddy current losses in insulated cables, *IEEE Transactions on Power Delivery*, Vol. 11, Issue 3, 1996, pp. 1171–1178.

[7]. T. K. Truong, Twisted-pair transmission-line distributed Parameters, *EDN Network*, 1969.

[8]. H. Meng, S. Chen, Y. Guan, C. Law, *et al*., A transmission line model for high-frequency power line communication channel, in *Proceedings of the Conference on Power System Technology (PowerCon'02),* Vol. 2, 2002, pp. 1290-1295.

[9]. P. Lefferson, Twisted magnet wire transmission line, *IEEE Transactions on Parts, Hybrids, and Packaging*, Vol. 7, Issue 4, 1971, pp. 148–154.

[10]. Kasthala S., Venkatesan G. P., Experimental verification of distributed parameters on Indian residential networks for power line communication, *International Journal of Engineering and Technology*, Vol. 8, Issue 6, 2016, pp. 2845–2852.

[11]. G. Smith, The proximity effect in systems of parallel conductors and electrically small multiturn loop antennas, Technical report, *Harvard Univ Cambridge Ma Div of Engineering and Applied Physics*, 1971.

[12]. P. B. Kahn, Mathematical methods for scientists and engineers: linear and nonlinear systems, *Courier Corporation*, 2004.

[13]. M. Kafal, J. Benoit, E. Cabanillas, Blind diagnosis of a black-boxed fully-loaded wiring network for configuration structuring and fault monitoring, in *Proceedings of the IEEE International Instrumentation and Measurement Technology Conference (I2MTC'18)*, 2018, pp. 1-6.

[14]. W. Ben Hassen, M. Kafal, E. Cabanillas, Time Reversal Applied to Multi-Carrier Reflectometry for On-line Diagnosis in Complex Wiring Systems, in *Proceedings of the IEEE AUTOTESTCON*, 2018.

[15]. W. Ben Hassen, M. Kafal, E. Cabanillas, A Stranded Unshielded Twisted Pair Modeling for Online Fault Location using OMTDR-based Diagnosis Sensor, in *Proceedings of the 8th International Conference on Sensor Networks (SENSORNETS'19),* Prague, Czech Republic, 26-27 February 2019, pp.40-46.